Diffusion-weighted magnetic resonance imaging of thymoma: ability of the Apparent Diffusion Coefficient in predicting the World Health Organization (WHO) classification and the Masaoka-Koga staging system and its prognostic significance on disease-free survival

Priola AM[1], Priola SM[1], Giraudo MT[4], Gned D, Fornari A[2], Ferrero M[3], Ducco L[1], Veltri A[1].

1 Department of Diagnostic Imaging, San Luigi Gonzaga University Hospital, Regione Gonzole 10, 10043 Orbassano (Torino), Italy
2 Department of Pathology, San Luigi Gonzaga University Hospital, Regione Gonzole 10, 10043 Orbassano (Torino), Italy
3 Department of Neurology, San Luigi Gonzaga University Hospital, Regione Gonzole 10, 10043 Orbassano (Torino), Italy
4 Department of Mathematics "Giuseppe Peano", University of Torino, Via Carlo Alberto 10, 10123 Torino, Italy

Diffusion-weighted magnetic resonance imaging of thymoma: ability of the Apparent Diffusion Coefficient in predicting the World Health Organization (WHO) classification and the Masaoka-Koga staging system and its prognostic significance on disease-free survival

Abstract

Objectives: To evaluate the usefulness of diffusion-weighted magnetic resonance for distinguishing thymomas according to WHO and Masaoka-Koga classifications and in predicting disease-free survival (DFS) by using the apparent diffusion coefficient (ADC).

Methods: Forty-one patients were grouped based on WHO (low-risk vs. high-risk) and Masaoka-Koga (early vs. advanced) classifications. For prognosis, seven patients with recurrence at follow-up were grouped separately from healthy subjects. Differences on ADC levels between groups were tested using Student-t testing. Logistic regression models and areas under the ROC curve (AUROC) were estimated.

Results: Mean ADC values were different between groups of WHO (low-risk=1.58±0.20×10-3mm2/sec; high-risk=1.21±0.23×10-3mm2/sec; p<0.0001) and Masaoka-Koga (early=1.43±0.26×10-3mm2/sec; advanced=1.31±0.31×10-3mm2/sec; p=0.016) classifications. Mean ADC of type-B3 (1.05±0.17×10-3mm2/sec) was lower than type-B2 (1.32±0.20×10-3mm2/sec; p=0.023). AUROC in discriminating groups was 0.864 for WHO classification (cut-point=1.309×10-3mm2/sec; accuracy=78.1 %) and 0.730 for Masaoka-Koga classification (cut-point=1.243×10-3mm2/sec; accuracy=73.2 %). Logistic regression models and two-way ANOVA were significant for WHOclassification (odds ratio[OR]=0.93, p=0.007; p<0.001), but not

for Masaoka-Koga classification (OR=0.98, p=0.31; p=0.38). ADC levels were significantly associated with DFS recurrence rate being higher for patients with ADC≤1.299× 10-3mm2/sec (p=0.001; AUROC, 0.834; accuracy=78.0 %).

Conclusions: ADC helps to differentiate high-risk from lowrisk thymomas and discriminates the more aggressive type-B3. Primary tumour ADC is a prognostic indicator of recurrence.

Key Points

• DW-MRI is useful in characterizing thymomas and in predicting disease-free survival.

• ADC can differentiate low-risk from high-risk thymomas based on different histological composition

• The cutoff-ADC-value of 1.309×10-3mm2/sec is proposed as optimal cut-point for this differentiation

• The ADC ability in predicting Masaoka-Koga stage is uncertain and needs further validations

• ADC has prognostic value on disease-free survival and helps in stratification of risk

Key Words: Thymoma .WHO classification . Masaoka-Koga staging system . Diffusion-weighted magnetic resonance imaging . Apparent diffusion coefficient

INTRODUCTION

Thymomas are benign or low-grade malignant tumours of the thymic epithelium and represent up to half of all neoplasms of the anterior mediastinum [1–6]. The histological classification proposed by the World Health Organization (WHO) and the Masaoka-Koga staging system, based on surgical findings, is currently used for treatment planning and significantly correlate with prognosis [1–8]. The Jeong simplification of WHO classification includes low-risk thymomas, high-risk thymomas, and thymic carcinomas [9]. The Masaoka-Koga system includes early (stage I–II) and advanced thymomas (stage III–IV) [8]. The correct prediction of early or advanced disease before surgery at imaging is essential to plan treatment strategies, because the latter receives neo-adjuvant chemotherapy [2]. Unfortunately, there is no perfect correlation among Jeong and Masaoka-Koga classifications because, although low-risk thymomas are frequently grouped in the earlydisease group, percentages of high-risk thymomas are reported at a rate up to 45 % in the early stage disease group [10]. Limited data are available on quantitative assessment of thymic epithelial tumours (TETs) by using diffusionweighted magnetic resonance imaging (DW-MRI) from small cohorts of studies which considered various anterior mediastinal tumours, although those studies did not attempt to differentiate thymomas based on WHO and Masaoka-Koga classifications by using the ADC [11–18]. More recently, a study involving 30 patients with TETs has demonstrated the ability of ADC in differentiating low-risk from high-risk tumours, and early from advanced disease [19]. Despite such promising results, that study is influenced by a strong correlation between Jeong and Masaoka-Koga classifications and by the inclusion of thymic carcinomas in the advanced disease group which leads to further decrease of the mean ADC value of this group compared with the early disease group [19, 20]. Moreover, perfusion-sensitive ADC values have been used for analyses by including the b value of 0 sec/mm2 for ADC computation, obtaining a measured signal which reflects not only pure molecular water diffusion, but also Bpseudo-diffusion^ resulting from fast-moving water molecules from blood flow in vessels and capillaries [21–25]. Hence, the ability of DWMRI in distinguishing thymomas based on WHO and

Masaoka-Koga classifications remains uncertain and optimal ADC cut-points should be validated. To date, no study has evaluated the predictive value of ADC of thymomas on disease-free survival (DFS) of patients with a thymoma for optimizing clinical decision making at diagnosis and improving patient care, although it is used as independent predictor of DFS and overall survival in different organs [23–25]. The aim of our study was to investigate the reliability of DW-MRI in predicting histological types of thymomas according to WHO classification, and whether DW-MRI can differentiate low-risk from high-risk thymomas, and early from advanced disease by using perfusion-freeADC measurements, with proposed optimal cut-point values for each differentiation. Moreover, we evaluated the prognostic value of ADC of a primary tumour for predicting DFS.

MATERIALS AND METHODS

Patient Population

An institutional review board approved the study, and informed consent was obtained from all subjects. In this prospective observational study conducted from January 2007 through December 2013, all subjects with generalized MG that underwent extended thymectomy or thymomectomy were considered eligible for inclusion. Five subjects were excluded for contraindications to MRI (cardiac pacemaker and claustrophobia, 3 subjects) and patient refusal to enrollment (2 subjects). Hence, 87 consecutive subjects (44 men, 43 women; all subjects: age range 15-71ys, median age 39ys, mean age ± standard deviation 38.6ys ± 11.8ys; male group: 18-68ys, 41ys, 40.6ys ± 20.1ys; female group: 15-71ys, 35ys, 36.5ys ± 13.0ys) were enrolled in this study and evaluated with MRI. The patients were assigned to two main groups based on the histological findings: a TLH/NT group (group A), that included 64 subjects, and a THY group (group B), that consisted of 24 patients (Table 1). One patient was listed in both groups because both TLH and non-advanced THY were found at histology after surgery (overall, 88 findings in 87 subjects). The mean age of patients in group A was lower than the mean age of those in group B and this age difference was statistically significant (36.5ys versus 44.2ys, respectively; p=0.009). For group B, according to the World

Health Organization (WHO) histological classification of thymic epithelial tumors, overall we found 4 type A, 3 type AB, 5 type B1, 6 type B2, and 6 type B3 tumors. The more aggressive type of THY, type B3, was more frequently found in advanced THY subgroup (non-advanced THY: 1 out of 15 cases, 6.7%; advanced THY: 5 out of 9 cases, 55.6%), and the significance of this difference was confirmed by performing the Fisher's exact test (p=0.015).

Proof of Diagnosis

The histologic and histopathologic results from surgical specimens were the standard reference for all subjects. For the 64 subjects of group A, a histological confirmation of TLH and NT was obtained through extended thymectomy; hence, 49 cases of TLH and 15 cases of NT were identified. For the 24 patients of group B, the diagnosis was pathologically established by surgical removal (thymomectomy plus extended thymectomy); thus, 15 cases of non-advanced THY (stage I-II, including the patient with THY and TLH) and 9 cases of advanced THY (stage III-IV) were found according to the Masaoka-Koga staging system (Table 1). The median time between MRI and surgery was 19 days (range, 1-35 days).

MR Imaging Protocol

All exams were performed using a 1.5T unit (Intera-Achieva, Philips Healthcare, Best, The Netherlands) with the manufacturer's 4-channel phased-array torso coil (Sense XL Torso; Philips Healthcare) for signal reception. MRI was performed to cover the entire chest, from the thoracic inlet to the cardiophrenic angle.

Chemical-shift MRI: All patients underwent transverse gradient-echo T1-weighted in- and opposed-phase imaging. The dual-echo acquisition, where both the in-phase and opposed-phase images were obtained in the same breath hold, was used for all patients. Other imaging parameters were as follows: 240-400 mm field of view, 256x256 image matrix, 5 mm section thickness, 0-0.5 mm intersection gap, flip angle 90^0, repetition time 154 msec, and in-phase and opposed-phase echo-times of 4.6 and 2.3 msec. For all exams, an anterior-to-posterior phase-encoding direction was used on the in-phase and opposed-phase images in order to avoid or minimize the presence of

artifacts within the anterior mediastinum (chemical-shift of the first kind or spatial misregistration) at the lipid-water interface between the thymus or the lesion on one hand, and the great vessels or the chest wall on the other. However, we used a left-to-right phase-encoding direction if artifacts were detected within the lesion by using the anterior-to-posterior phase-encoding direction (i.e. large masses that widely protruded from the left or right side of the mediastinum).

Diffusion-weighted MRI: DW imaging was performed using a single-shot spin-echo echo-planar sequence with the following parameters: 360-500 mm field of view, 116x224 image matrix, 45 echo planar imaging factor, 5 mm slice thickness, 0.5 mm intersection gap, 1600 msec repetition time, 62 msec echo time, 1600 Hz/pixel bandwidth. Four signals were acquired per image with diffusion sensitizing gradients applied in three orthogonal planes (*x*, *y*, and *z*), in order to obtain isotropic diffusion weighting, and *b* values of 0, 150, 500, and 800 sec/mm^2. All sequences were performed using a parallel imaging technique acquisition and SENSE (sensitivity encoding) reconstruction with a reduction factor (*R*) of 2. Fat was suppressed by placing a frequency-selective radiofrequency pulse before the pulse sequence.

MR Image Analysis

All exams were analyzed independently for qualitative and quantitative assessment by two radiologists (A.M.P. and D.G., each with 8 years of experience in thoracic MRI) who were unaware of the patients' identification and clinical data. The image analysis was performed by using a Windows workstation (Dell, Xeon CPU 3.20 GHz) with dedicated software (Extended MR WorkSpace, version 2.6.3.1, 2009; Philips Healthcare, Best, The Netherlands).

Chemical-shift MRI: For qualitative assessment, the readers determined whether the decrease in signal intensity of the thymus or the lesion was seen on the opposed-phase images relative to the in-phase images. For quantitative assessment, the signal intensity measurements within the thymus or the mass were obtained with an electronic cursor, using regions of interest (ROI) of the same size, that was placed over the same position within the tissue on both in-phase and opposed-phase images in each case. The selection of the ROI placement was first made on the opposed-phase image, in

order to avoid the inclusion of areas of signal void at the interfaces between the fat-dominant and water-dominant tissues (India ink artifact), and then mirrored on the in-phase image in the exact same position. On the opposed-phase T1-weighted image, the readers placed the ROI within the anterior mediastinal soft tissue that exhibited the highest signal intensity, avoiding cystic, necrotic, or calcified components. The SII was determined by comparing the signal intensity of the thymic tissue (tSI) on both in-phase (in) and opposed-phase (op) images by using the following equation: $SII=[(tSI_{in}–tSI_{op})/(tSI_{in})]x100\%$.

Diffusion-weighted MRI: For qualitative assessment, the readers determined whether, in the thymus or the lesion, a persistent high signal or a signal attenuation were detected on images obtained with the higher *b* value of 800 s/mm^2 or whether a complete signal suppression occurred at the lower *b* values of 150 or 500 s/mm^2. For quantitative assessment, the ADC maps were reconstructed from the *b* 150, 500, and 800 s/mm^2 images. The *b* 0 s/mm^2 images were excluded from the reconstruction of the ADC maps and thus from the ADC computation to suppress tissue perfusion (the perfusion bias or "intravoxel incoherent motion") in order to obtain perfusion-insensitive ADC values by eliminating the vascular contribution to the calculated ADC which would lead to an increase of the ADC value.[13-15] For each patient, all the axial sections that included the lesion or the thymus (from 3 to 32 slices) were identified by using both DW sequences and ADC maps, chemical-shift images, and conventional T2-weighted images with and without fat suppression. Within each of these sections on the ADC maps, a ROI was defined using an electronic cursor along the circumference of the lesion or thymus, but within the boundaries. The ROI was manually drawn to include only the solid portion of the tissue, taking care to exclude obvious cystic and/or necrotic areas which were identified on the corresponding conventional T2-weighted images. The median ADC was calculated from all the ADC values obtained at each axial section of the tissue for each case and was used for further analyses.

Statistical Analysis

The Shapiro-Wilk test was performed and showed that the data were parametric with normal distribution. Hence, all data concerning SII and ADC levels, according to the defined groups and subgroups, were expressed as mean values ± standard deviations and ranges. Furthermore, they were also represented using box and whiskers plots. The inter-reader agreement of SII and ADC measurements was assessed by using the intraclass correlation coefficient (ICC, range: from 0 [no agreement] to 1 [perfect agreement]), calculated between the two readers. The SII and ADC values were then compared between groups and subgroups. The differences in SII and ADC levels between groups and subgroups were analyzed using the parametric Student-*t* test. Logistic regression models were estimated in order to evaluate the ability of SII and ADC levels to discriminate between groups (TLH/NT vs. THY) and between subgroups of group A (TLH vs. NT). The discrimination abilities were evaluated by the Area Under the Receiver Operating Characteristic (ROC) curve (AUROC) that was used to find the optimal SII and ADC cut-points. The optimal cut-points were determined according to the Youden Index with computation of sensitivity and specificity. Additional analyses aimed to control for age as a potential confounding factor were performed by including the age in logistic regression models. Furthermore, the correlation between both the quantitative parameters (SII and ADC) with age was evaluated by using the Pearson's correlation coefficients. A *p* value of less than 0.05 was considered indicative of a statistically significant difference. All statistical analyses were performed with "R" software package (release 3.0.2; The R Foundation for Statistical Computing) .

RESULTS

Reliability of MRI in assessing the correct diagnosis

One out of 87 cases with histological diagnosis of microscopic foci of TLH after extended thymectomy was excluded from the SII and ADC measurements because MRI demonstrated fatty involution of the thymus with no islands of soft tissue attenuation in the anterior mediastinum. Moreover, one subject was listed in both groups (A and B) because histology demonstrated non-

advanced THY and TLH, an association that was correctly suspected on chemical-shift MRI. Thus, MRI was able to define the correct diagnosis in 98.85% of cases (86 out of 87 subjects) in our cohort of patients with generalized MG that underwent surgery during the enrollment period. Nevertheless, MRI was able to differentiate perfectly between THY and benign conditions (TLH and NT) in all patients.

Interobserver variability for quantitative and qualitative assessment

For quantitative evaluations, the inter-reader agreement regarding both SII and ADC measurements was excellent with an ICC near to 1. The estimation of ICCs were 0.998 (95% confidence interval [95%CI]: 0.998-0.999) and 0.944 (95%CI: 0.915-0.963) for SII and ADC, respectively. Therefore, the mean SII and ADC value of the two readers was calculated for each case and used for further analyses.

For qualitative evaluations, there was a perfect concordance between the two readers in assessing the presence or absence of signal intensity loss on opposed-phase images compared to in-phase images at chemical-shift MRI for all cases. Furthermore, a perfect concordance was also found in evaluating the complete signal suppression on DW images at different *b* values of 150, 500 and 800 s/mm^2 or the signal intensity persistence at the higher *b* value of 800 s/mm^2. Hence in both cases it was not necessary to compute a statistical index of concordance.

Quantitative analysis: differences of SII and ADC between groups and subgroups

The mean values ± standard deviations of SII and ADC for the TLH/NT group (group A) and THY group (group B), and for subgroups of each group are reported in Table 2. For groups, the SII and ADC differed significantly between the two groups ($p<0.001$ for both quantitative parameters). For subgroups of each group, by evaluating the SII, no significant differences between subgroups were found in both groups (group A, $p=0.607$; group B, $p=0.252$). Conversely, the ADC was significantly different between subgroups of each group (group A, $p=0.002$; group B, $p<0.001$). Figures 1a and 1b show the box plots comparing the SII and ADC values for group A with those of group B, respectively.

The logistic regression model for SII was not estimable since the value of 6.37% predicts group perfectly, with no overlap in range between groups (Figs. 1a and 1c), with an AUROC of 1.000. Thus, considering 6.37% as cut-point, for the diagnosis of THY and its differentiation from TLH and NT, sensitivity was 100% (24/24) and specificity was 100% (63/63).

For DW-MRI, considering the logistic regression model for groups A and B, the tumor probability decreased with the increase of ADC (Odds Ratio [OR] *per* 0.01 increase, 0.91; 95%CI: 0.86-0.94). AUROC of ADC in discriminating between groups was 0.931 (95%CI: 0.863-0.998) (Fig. 2a). The optimal cut-point was identified in ADC value of 1.625 x $10^{-3}mm^2s^{-1}$ (Youden Index J=0.760). Applying this cut-point, for the diagnosis of TLH/NT, sensitivity was 96.8% (61/63, 95%CI: 92.7-100) and specificity was 79.2% (19/24, 95%CI: 62.4-95.7). In the logistic model adjusted for age, OR was 0.89 *per* 0.01 ADC increase (95%CI: 0.83-0.94). Overlapped ADC values between group A and B were found in the range from 1.52 to 2.01 x $10^{-3}mm^2s^{-1}$ for 43 out of 63 (68.2%) subjects of group A and for 7 out of 24 (29.2%) patients of group B (Fig. 1b).

For DW-MRI, considering the logistic regression model for subgroups of group A (TLH and NT), the probability of finding a NT increased with the increase of ADC (Odds Ratio [OR] *per* 0.01 increase, 1.06; 95%CI: 1.03-1.11). AUROC of ADC in discriminating between subgroups of group A was 0.794 (95%CI: 0.666-0.923) (Fig. 2b). The optimal cut-point was identified in ADC value of 2.01 x $10^{-3}mm^2s^{-1}$ (Youden Index J=0.458). Applying this cut-point, for the diagnosis of NT, sensitivity was 66.7% (10/15, 95%CI: 42.7-75.7) and specificity was 79.2% (38/48, 95%CI: 67.2-90.8). In the logistic model adjusted for age, OR was 1.10 *per* 0.01 ADC increase (95%CI: 1.05-1.17). Overlapped ADC values between NT and TLH were found in the range from 1.79 to 2.25 x $10^{-3}mm^2s^{-1}$ for 11 out of 15 (73.3%) subjects of NT subgroup and for 28 out of 48 (58.3%) subjects of TLH subgroup (Fig. 1d).

Quantitative analysis: relationship between SII-ADC and age

We analyzed the correlation between both the quantitative parameters and the age of patients in order to search for potential influences of age on SII and ADC values. Figure 3 shows this

relationship for each group. For chemical-shift MRI, when age was tested for its correlation with SII, a high significant positive correlation was found for group A (r=0.885, $p<0.0001$), but not for group B (r=0.245, $p=0.249$) (Figs. 3a and 3b, respectively); for DW-MRI, a mild positive correlation was found between ADC and age for group A (r=0.288, $p=0.022$), whereas the ADC did not vary with age in group B (r=0.235, $p=0.269$) (Figs. 3c and 3d, respectively).

Qualitative analysis

Chemical-shift MRI: at qualitative analysis, for group A, a homogeneous decrease in signal intensity of the thymus was detected on opposed-phase images relative to in-phase images in 61 out of 63 (96.8%) subjects, namely in all patients of the NT subgroup (age range, 18-49ys), and in all patients but two of the TLH subgroup (age range, 15-71ys) (Fig. 4a). The two cases with no signal intensity loss visually appreciable on opposed-phase images were a 15-year-old woman and a 23-year-old man (SII of 7.77% and 12.66%, respectively), in which histology proved minimally fatty-infiltrated thymic tissue with many lymphoid follicles (Fig. 5a). No signal intensity loss was detected on opposed-phase images in any patients in the THY group (Fig. 6a). In addition, chemical-shift MRI successfully revealed a small rounded THY embedded in TLH in a 39-year-old man (SII of 0.64% with no decrease in signal intensity and 31.79% with signal intensity loss, respectively).

Diffusion-weighted MRI: For group A, the ADC map demonstrated unrestricted diffusion by showing homogeneous bright appearance of the thymus in all subjects (Figs. 4b and 5b). In the same group, on native DW images obtained at different *b* values, a complete signal suppression was seen at the low *b* value of 150 s/mm^2 in 52 out of 63 subjects (82.5%; 38/48 cases for TLH and 14/15 cases for NT), at the intermediate *b* value of 500 s/mm^2 in 11 out of 63 subjects (17.5%; 10/48 cases for TLH and 1/15 cases for NT), but in none a persistent high or attenuated signal was maintained at the higher *b* value of 800 s/mm^2 (Figs. 4c and 5c). For group B, the ADC map revealed homogeneous or inhomogeneous hypointensity within the lesion suggestive for restricted diffusion with no complete signal suppression at the higher *b* value of 800 s/mm^2 in all cases (Fig. 6b-c) but one. This last case (type AB THY) demonstrated complete signal suppression on the

image obtained at *b* 800 s/mm^2 with areas of bright appearance suggestive for unrestricted diffusion on the ADC map (ADC of 2.01 x 10^{-3}mm^{2}s^{-1}).

DISCUSSION

MG is an autoimmune disorder of the neuromuscular junction characterized by muscle weakness, often initially involving the extrinsic ocular muscles and subsequently resulting in generalized MG in two-thirds of patients.[1] The thymus has a role in the pathogenesis of MG that is highlighted by the presence of frequent histological abnormalities in patients with generalized MG, namely TLH and THY, and by the clinical benefit after thymectomy in certain conditions.[16] Diagnostic imaging is crucial in all patients affected by MG for evaluating the presence of an underlying TLH or THY and for distinguishing these two conditions in order to select the proper therapeutic management, because the treatment strategies are different.[2,16,17] Indeed, surgery is strongly recommended in patients with THY and represents the mainstay of the curative-intent treatment, since complete resection is the most significant positive prognostic factor, both on disease-free and overall survival.[18] Conversely, in non-thymomatous MG, the primary therapeutic management is based on the use of acetylcholinesterase inhibitors and immunomodulatory agents.[1] Lastly, an accurate imaging technique to differentiate THY from non-thymomatous conditions (TLH, NT, and atrophic thymus) is also required because, in a recent survey of current practice among members of the European Society of Thoracic Surgeons, 91% of centers declared to not routinely look for preoperative histological confirmation when CT strongly suggests a small thymoma with no apparent signs of invasion, especially if MG is associated.[18]

CT is currently considered the cross-sectional imaging technique of choice in the evaluation of patients with MG.[2,4,19] At CT, differentiation of TLH from THY is mostly based on morphological and attenuation assessment because a normal CT appearance or a diffuse symmetric enlargement of the thymus with areas of fat attenuation represent the key morphologic features of hyperplasia (or even normal thymus if normal-sized), whereas a diagnosis of thymoma is suggested if a solid focal

mass rather than a normal or diffusely enlarged thymus is detected.[2] However, CT has limitations in distinguishing TLH from THY when TLH appears as a focal mass with homogeneous soft-tissue attenuation and no clear fatty infiltration, a condition that has been reported in 20% of cases in a cohort of 45 patients with MG.[4]

Currently, MRI is not routinely employed in the evaluation of patients with MG, although it can provide more specific characterization compared to CT, especially in differentiating TLH from THY, regardless of morphologic assessment, by using chemical-shift imaging.[2] Indeed, chemical-shift MRI is able to detect microscopic fatty infiltration within the normal/hyperplastic thymus, which would be indistinct at CT, by showing homogeneous signal decrease on opposed-phase images relative to in-phase images, whereas signal loss is absent in THY that does not include fat.[6,20-22] Nevertheless, only two previous studies with small sample size have used chemical-shift MRI to evaluate TLH and THY in patients with MG (overall, 15 patients: 5 TLH, 9 THY).[6,7] Those studies demonstrated that all cases of TLH showed signal intensity loss on opposed-phase images, but none of patients with THY.[6,7] Conversely, for qualitative assessment, in our cohort, we found no signal intensity loss on opposed-phase images in all patients with THY (as seen in previous studies) and in two cases of TLH, that were a 15-year-old girl and a 23-year-old man with minimally fatty-infiltrated TLH at histology. For children and adolescents, this finding is consistent with a previous study that evaluated the fatty replacement of the normal thymus with chemical-shift MRI in 95 healthy volunteers.[20] Those investigators found that chemical-shift MRI can detect physiological fatty infiltration of the normal thymus in all subjects ≥16 years, in half of adolescents aged 10-16 years, but in none <10 years, although a microscopic and gradually increasing amount of fat in the normal thymus exists from birth.[20] In addition, a recent report described a case of non-suppressing normal thymus in a 21-year-old woman.[23] Thus, similarly to the normal thymus, cases of non-suppressing TLH at chemical-shift MRI may also occur in patients with MG, even in early adulthood, as seen in our study. Despite the imperfect reliability of chemical-shift MRI by visual assessment in distinguishing TLH from THY, by using SII for quantitative evaluation, we found no

overlap in range of SII values between the two groups (TLH/NT versus THY) and a signal intensity loss of 7.77% or greater for TLH/NT group. In addition, the mean SII was significantly higher in TLH/NT group compared to THY group. Previous studies did not measure the SII in evaluating thymic abnormalities, because they did not use dual-echo single-breath-hold acquisition for chemical-shift imaging.[6,7] Thus, the in-phase and opposed-phase images were separately obtained at chemical-shift MRI, and the signal intensity of the thymic abnormality (TLH and THY) or normal thymus was compared with that of the paraspinal muscles or chest wall muscles by using the chemical shift ratio (CSR) to assess any drop-out in signal intensity of the thymus between the two images.[6,7,20] However, the CSR measurement, which is normalized to the paraspinal musculature, could be affected by age and body mass index, since subjects lose muscle mass as they age and the muscle has more fat interspersed between the muscle fiber bundles in older and/or overweight subjects.[6,24] For this reason, in the present study, we preferred the use of dual-echo chemical-shift MRI, which does not require any normalization for its calculation, as used in previous studies for differentiating adrenal adenomas from non-adenomas.[8,24] By using dual-echo chemical-shift MRI, considering the SII, we found a sensitivity and specificity of 100% in distinguishing TLH and NT from THY. Furthermore, in our study, quantitative evaluation was more accurate than qualitative analysis. Indeed, the two cases of TLH with no signal intensity loss at visual assessment had a signal intensity loss of 7.77% and 12.66% at quantitative evaluation. Hence, quantitative evaluations should always be performed in chemical-shift MRI, because qualitative analysis may be less sensitive than quantitative analysis for the characterization of TLH.

DW-MRI did not show the perfect predictive ability of chemical-shift MRI for distinguishing TLH and NT from THY. Indeed, in the present study, we demonstrated a sensitivity of 96.8% and a specificity of 79.2% for this differentiation with an optimal ADC cut-point of $1.625 \times 10^{-3} mm^2 s^{-1}$, because an overlap in range of ADC values between groups was found. Nevertheless, the mean ADC value of TLH/NT group was significantly higher than that of THY group. Similarly to DW imaging studies in other oncologic applications, the ability of differentiating tumors from benign

conditions is most likely due to the increased cellular density and vascularity in thymic epithelial tumors compared to TLH and NT (in which the variable fatty infiltration leads to a decrease of cell density), a condition that causes restriction to diffusion.[25] To date, no study evaluated the ability of DW-MRI in differentiating TLH and NT from THY, and no data are reported on the characterization of NT (and relative ADC values) at DW imaging. Conversely, for THY and thymic hyperplasia, few data are available based on a limited number of patients enrolled in two different studies.[10,11] Abdel Razek and colleagues demonstrated a lower mean ADC in eight patients with invasive THY compared to three cases of non-invasive THY ($1.10\pm0.18 \times 10^{-3} mm^2 s^{-1}$ and $2.00\pm0.11 \times 10^{-3} mm^2 s^{-1}$, respectively).[11] Subsequently, in the study of Gumustas and colleagues, two cases of non-invasive THY and five cases of thymic hyperplasia were included, both grouped under benign conditions.[10] Although they did not report the type of hyperplasia (rebound or lymphoid) nor the mean ADC value of each subgroup in benign group, the mean value for all 27 benign lesions (that included various conditions) was $2.04\pm0.67 \times 10^{-3} mm^2 s^{-1}$.[10] For non-advanced THY, we found lower ADC values (mean value, $1.53\pm0.25 \times 10^{-3} mm^2 s^{-1}$) compared to those reported for non-invasive THY in previous studies.[10,11] This discordance could be related to the "perfusion bias" with a consequent overestimation in ADC measurements of those studies. Indeed, as both the investigators used also the images obtained with *b* values of 0 s/mm^2 for the ADC computation, the ADC value was determined not only by diffusion (related to cell density and cellular architecture) but also by tissue perfusion. Blood flow may determine significant signal attenuation over the low *b*-value range (from 0 to 100 s/mm^2), which artificially inflates diffusion estimates and thus may be mistakenly attributed to diffusion.[13,25-28]

In contrast with Abdel Razek, that distinguished Masaoka-Koga stage I disease (non-invasive THY) from higher stages (II-IV, invasive THY), we assessed whether DW-MRI could distinguish stage I-II (non-advanced THY, no neo-adjuvant therapy before surgery required), from stage III-IV (advanced THY, neo-adjuvant treatments needed).[11] Although we found a significantly higher mean ADC in non-advanced THY compared to advanced THY, this finding may have been influenced by

the higher percentage of type B3 THY in advanced THY subgroup (56% versus 7% of non-advanced THY subgroup). Indeed, the lower ADC values generally found in malignant tumors compared to benign conditions are related to a combination of higher cell density, tissue disorganization, and increased extracellular space tortuosity, all contributing to reduced motion of water.[13,25] On these basis, lower ADC values can be expected in type B3 THY that is typically characterized by a prominent population of medium-sized polygonal epithelial cells and is the only histological type of THY that presents nuclear atypia and prominent nucleoli.[29] This finding is similar to that obtained in a recent study by Benveniste and colleagues that evaluated the ability of 2-[^{18}F]-fluoro-2-deoxy-D-glucose (FDG) positron emission tomography (PET)-CT in differentiating non-advanced from advanced THY and THY from thymic carcinoma.[30] Although no significant association was observed between higher focal FDG uptake and advanced THY, they found that FDG PET-CT is helpful in distinguishing thymic carcinoma and the more aggressive type B3 THY from the other histological types of THY.[30]

Albeit chemical-shift MRI is highly accurate in distinguishing TLH and NT from THY, it is not useful in differentiating TLH from NT. Indeed, in our study, the mean SII was not different between subgroups of group A (TLH and NT). This finding proves that the lipid content of the thymus is not different among TLH and NT in subjects of the same age group. In addition, in MG patients, TLH is morphologically indistinguishable from a NT when it has normal size for a given patient's age and exhibits the typical triangular shape, a condition that occurs in 45% of MG patients with TLH.[4] The distinction between TLH and NT would be beneficial in patients with non-thymomatous MG and anti-AChR antibodies in order to select appropriately patients for surgery. Indeed, in non-thymomatous MG, the clinical efficacy of thymectomy has been questioned because the evidence supporting its use is not clear and has largely been based on single-institution retrospective, observational studies.[3] Currently, although no uniformly accepted guidelines are available, thymectomy is believed to be suitable for patients with generalized MG under 50 years with anti-AChR antibodies and TLH, as an option to increase the probability of clinical improvement or

complete stable remission.[16] Contrariwise, effectiveness of extended thymectomy is still under discussion in patients with generalized MG and atrophic thymus or histological NT because the results of different studies are controversial, and stable remission rates up to 10 years of follow-up are significantly higher in TLH compared to NT or atrophic thymus in the majority of studies.[3,4] To date, no study characterized the NT with DW imaging nor evaluated the ability of DW-MRI in differentiating TLH from NT. In the present study, the mean ADC of TLH was significantly lower than that of NT, although overlapped values were found. The lower ADC of TLH is probably related to its higher cellular density compared to NT, even for the presence of lymphoid germinal centres in the thymic medulla. Furthermore, a recent study by Matsui and colleagues demonstrated that the number of Hassall's corpuscles per unit area of the thymic medulla is significantly higher in the thymuses of MG patients with TLH compared to MG patients with NT or THY.[12] This new evidence suggests, once again, a higher cellular density and an increased number of prominent cells in TLH compared to NT that could explain the lower ADC values found in TLH.

Another interesting finding of our research is the positive correlation between the quantitative parameters evaluated (SII and ADC) and age of patients in TLH/NT group. For chemical-shift MRI, it suggests a different amount of fatty tissue within the thymus that increases with age; for DW-MRI, it is related to a gradually decreased cellular density in the thymus while age increases. Although these results are expected for the normal thymus and explained by the progressive fatty replacement and atrophy of the thymus with age, these findings could reflect for TLH a greater response of the thymus under the associated conditions (mostly autoimmune diseases, as MG) in younger subjects, with a lower amount of fat and an increased cellular density (lymphoid germinal centres and Hassall's corpuscles) within the thymus, compared to elderly patients.

Albeit chemical-shift MRI demonstrated a perfect reliability in differentiating THY from TLH and NT in our cohort, even in associated conditions of TLH and THY in the same patient, we found one case of discordance between MRI and histology. Indeed, in this case, while chemical-shift and DW-MRI showed a thymus as entirely replaced by fat and classified as atrophic, the histological

examination after thymectomy (surgery performed for clinical reasons and patient's decision) diagnosed microscopic foci of TLH. Hence, MRI could have limitations for detecting microscopic foci of TLH and THY that are indistinguishable from mediastinal fat.

The present study has some limitations. First, during the enrolment period, we did not include in our cohort all consecutive patients with onset of generalized MG, but only all consecutive patients that underwent surgical resection of the thymus in order to have histological examination as reference standard of diagnosis for all cases. This did not allow us to accurately assess sensitivity and specificity of MRI for detecting thymic abnormalities because patients with an atrophic thymus at CT and MRI, that were excluded from surgery, were not enrolled. Thus, we may have excluded other patients with microscopic foci of TLH or THY that presented an atrophic thymus at MRI. However, our primary endpoint was to evaluate the accuracy of MRI in differentiating TLH, NT and THY in patients with detectable thymic abnormalities. Second, we did not evaluate the cell count of a representative tissue block for each case in order to determine the number of cell/mm^2. The demonstration of a significant negative correlation between cellularity and ADC in TLH/NT group, with higher ADC values for elderly patients compared to early adulthood, would have confirmed that cellular density in TLH decreases with increasing age.

In conclusion, both chemical-shift MRI and DW-MRI are helpful tools for the evaluation of patients with generalized MG. The SII is a more accurate quantitative parameter than the ADC for distinguishing THY from TLH and NT. Nevertheless, for patients with non-thymomatous MG and anti-AChR antibodies, DW-MRI could represent an useful non-invasive method to differentiate non-enlarged TLH from NT in order to select appropriately patients for surgery, thus increasing chance of clinical improvement and complete stable remission.

REFERENCES

1. Silvestri NJ, Wolfe GI. Myasthenia gravis. Semin Neurol. 2012;32:215-226.

2. Priola AM, Priola SM. Imaging of thymus in myasthenia gravis: from thymic hyperplasia to thymic tumor. Clin Radiol. 2014;69:e230-245.
3. Diaz A, Black E, Dunning J. Is thymectomy in non-thymomatous myasthenia gravis of any benefit? Interact Cardiovasc Thorac Surg. 2014;18:381-389.
4. Nicolau S, Muller NL, Li DKB, et al. Thymus in myasthenia gravis: comparison of CT and pathologic findings and clinical outcome after thymectomy. Radiology. 1996;200:471-474.
5. Priola AM, Priola SM. Chemical-shift MRI of rebound thymic hyperplasia with unusual appearance and intense ^{18}F-FDG uptake in adulthood: report of two cases. Clin Imaging. 2014;38:739-742.
6. Inaoka T, Takahashi K, Mineta M, et al. Thymic hyperplasia and thymus gland tumors: differentiation with chemical shift MR imaging. Radiology. 2007;243:869-876.
7. Popa GA, Preda EM, Scheau C, et al. Updates in MRI characterization of the thymus in myasthenic patients. J Med Life. 2012;5:206-210.
8. Park BK, Kim CK, Kim B, et al. Comparison of delayed enhanced CT and chemical shift MR for evaluating hyperattenuating incidental adrenal masses. Radiology. 2007;243:760-765.
9. Lichy MP, Aschoff P, Plathow C, et al. Tumor detection by diffusion-weighted MRI and ADC-mapping--initial clinical experiences in comparison to PET-CT. Invest Radiol. 2007;42:605-613.
10. Gümüştaş S, Inan N, Sarisoy HT, et al. Malignant versus benign mediastinal lesions: quantitative assessment with diffusion weighted MR imaging. Eur Radiol. 2011;21:2255-2260.
11. Abdel Razek A, Elmorsy A, Elshafey M, et al. Assessment of mediastinal tumors with diffusion weighted single shot echo planar MR imaging. J Magn Reson Imaging. 2009;30:535-540.

12. Matsui N, Ohigashi I, Tanaka K, et al. Increased number of Hassall's corpuscles in myasthenia gravis patients with thymic hyperplasia. J Neuroimmunol. 2014;269:56-61.
13. Padhani AR, Guoying L, Mu-Koh D, et al. Diffusion-weighted magnetic resonance imaging as a cancer biomarker: consensus and recommendations. Neoplasia. 2009;11:102-125.
14. Priola AM, Priola SM. Influence of selected b values on ADC quantification in diffusion-weighted MRI. Comment on Punwani et al.: Diffusion-weighted MRI of lymphoma: prognostic utility and implications for PET/MRI? Eur J Nucl Med Mol Imaging. 2013;40:1108-1109.
15. Hwang EJ, Lee JM, Yoon JH, et al. Intravoxel incoherent motion diffusion-weighted imaging of pancreatic neuroendocrine tumors: prediction of the histologic grade using pure diffusion coefficient and tumor size. Invest Radiol. 2014;49:396-402.
16. Lewis RA. Myasthenia gravis: new therapeutic approaches based on pathophysiology. J Neurol Sci. 2013;333:93-98.
17. Priola AM, Priola SM, Cardinale L, et al. The anterior mediastinum: diseases. Radiol Med. 2006;111:312-342.
18. Ruffini E, Van Raemdonck D, Detterbeck F, et al. European Society of Thoracic Surgeons Thymic Questionnaire Working Group. Management of thymic tumors: a survey of current practice among members of the European Society of Thoracic Surgeons. J Thorac Oncol 2011;6:614-623.
19. Priola SM, Priola AM, Cardinale L, et al. The anterior mediastinum: anatomy and imaging procedures. Radiol Med. 2006;111:295-311.
20. Inaoka T, Takahashi K, Iwata K, et al. Evaluation of normal fatty replacement of the thymus with chemical-shift MR imaging for identification of the normal thymus. J Magn Reson Imaging. 2005;22:341-346.

21. Priola AM, Priola SM. Primary mediastinal Hodgkin lymphoma and rebound thymic hyperplasia: differentiation with chemical-shift magnetic resonance imaging after treatment. Int J Hematol. 2009;90:8-10.
22. Kang BK, Yu ES, Lee SS, et al. Hepatic fat quantification: a prospective comparison of magnetic resonance spectroscopy and analysis methods for chemical-shift gradient echo magnetic resonance imaging with histologic assessment as the reference standard. Invest Radiol. 2012;47:368-375.
23. Ackman JB, Mino-Kenudson M, Morse CR. Nonsuppressing normal thymus on chemical shift magnetic resonance imaging in a young woman. J Thoracic Imaging. 2012;27:196-198.
24. Priola AM, Priola SM, Ciccone G, et al. Differentiation of rebound and lymphoid thymic hyperplasia from anterior mediastinal tumors with dual-echo chemical-shift magnetic resonance imaging in adulthood: reliability of the chemical-shift ratio and signal-intensity index. Radiology. 2014; DOI: 10.1148/radiol.14132665.
25. Padhani AR, Koh DM, Collins DJ. Whole-body diffusion-weighted MR imaging in cancer: current status and research directions. Radiology. 2011;261:700-718.
26. Concia M, Sprinkart AM, Penner AH, et al. Diffusion-weighted magnetic resonance imaging of the pancreas: diagnostic benefit from an intravoxel incoherent motion model-based 3 b-value analysis. Invest Radiol. 2014;49:93-100.
27. Chandarana H, Kang SK, Wong S, et al. Diffusion-weighted intravoxel incoherent motion imaging of renal tumors with histopathologic correlation. Invest Radiol. 2012;47:688-696.
28. Priola AM, Galetto G, Priola SM. Diagnostic and functional imaging of thymic and mediastinal involvement in lymphoproliferative disorders. Clin Imaging. 2014; DOI: 10.1016/j.clinimag.2014.05.012.
29. Priola AM, Priola SM, Di Franco M, et al. Computed tomography and thymoma: distinctive findings in invasive and noninvasive thymoma and predictive features of recurrence. Radiol Med. 2010;115:1-21.

30. Benveniste MF, Moran CA, Mawlawi O, et al. FDG PET-CT aids in the preoperative assessment of patients with newly diagnosed thymic epithelial malignancies. J Thorac Oncol 2013;8:502-510.

Tables

Table 1. Demographic Characteristics of the 87 Evaluated Patients [§]

Group and Subgroup	n [§]	M/F ratio	Age (years)*	Size (mm)**
Non-thymomatous conditions (group A)	64	30/34	36.5 [11.0]	12.6 [4.2] [§§]
Thymic lymphoid hyperplasia [§]	49	23/26	37.6 [11.0]	13.7 [4.0] [§§]
Normal thymus	15	7/8	33.1 [10.8]	8.9 [2.2]
Thymomas (group B)	24	15/9	44.2 [11.9]	36.9 [26.6]
Non-advanced thymoma ***/[§]	15	9/6	44.1 [12.1]	23.0 [11.5]
Advanced thymoma ***	9	6/3	44.3 [12.4]	60.1 [28.9]

n = number of patients; M = male; F = female.
*/** Data are mean values [standard deviation].

** Size is the thickness of the thymus gland measured as the maximum dimension perpendicular to the long axis of each lobe for group A and the maximal diameter of the lesion for group B, measured on transverse images.
*** Non-advanced thymoma = Masaoka-Koga stage I-II; advanced thymoma = Masaoka-Koga stage III-IV.
§ One subject is listed in both groups (final diagnosis of thymic lymphoid hyperplasia and non-advanced thymoma in the same patient after thymomectomy and extended thymectomy).
§§ Mean size obtained in 63 out of 64 patients (for group A) and in 48 out of 49 patients (for thymic lymphoid hyperplasia subgroup) after excluding one subject with a MRI appearance of complete fatty involution of the thymus (histological finding of microscopic foci of thymic lymphoid hyperplasia after extended thymectomy).

Table 2. Mean SII and ADC of Groups A and B with Subgroups

Parameter	**Groups or Subgroups**		**p**
	Group A [63$^{§/§§}$]	**Group B [24§]**	
SII (%)*	36.37±12.60 (7.77/66.11)	-0.06±3.85 (-7.95/6.37)	<0.001
ADC (x $10^{-3}mm^2s^{-1}$)*	1.92±0.21 (1.52/2.53)	1.36±0.33 (0.72/2.01)	<0.001
Group A	**Thymic Lymphoid Hyperplasia [48$^{§/§§}$]**	**Normal Thymus [15]**	
SII (%)*	35.51±12.51 (7.77/60.40)	37.94±13.61 (15.69/66.11)	0.607
ADC (x $10^{-3}mm^2s^{-1}$)*	1.86±0.17 (1.52/2.25)	2.10±0.23 (1.79/2.53)	0.002
Group B	**Non-advanced Thymoma** [15§]**	**Advanced Thymoma** [9]**	
SII (%)*	-0.81±3.56 (-7.95/5.27)	1.18±4.20 (-5.13/6.37)	0.252
ADC (x $10^{-3}mm^2s^{-1}$)*	1.53±0.25 (1.13/2.01)	1.09±0.24 (0.72/1.48)	<0.001

A = thymic hyperplasia/normal thymus group; B = tumor group; numbers in square brackets are number of patients.
* Data are mean values ± standard deviations. Numbers in brackets are ranges.
** Non-advanced thymoma = Masaoka-Koga stage I-II; advanced thymoma = Masaoka-Koga stage III-IV.
§ One subject is listed in both groups (MRI appearance of thymoma associated with thymic hyperplasia/normal thymus, confirmed after surgical removal).
§§ One subject with final diagnosis of microscopic foci of thymic lymphoid hyperplasia is excluded from the SII and ADC measurements because of the MRI appearance of complete fatty involution of the thymus.

FIGURE LEGENDS

FIGURE 1. Box-and-whiskers plots show the SII (a,c) and ADC (b,d) values for all cases divided into groups (a,b) and subgroups (c,d). The subgroups include subjects with thymic lymphoid hyperplasia (TLH) and normal thymus (NT) for group A, and patients with advanced thymoma (ATHY) and non-advanced thymoma (NATHY) for group B. The boxes represent data from the

25^{th} to the 75^{th} percentile. The horizontal line inside the boxes is the median (50^{th} percentile). The vertical lines with whiskers indicate the range from the largest to smallest observed data point, within 1.5xIQR of the higher and lower quartile, respectively. The value outside this range (group A, NT) is displayed as an individual point. The continuous horizontal thick line in the graphs shows the optimal cut-point value for discrimination among groups deriving from the ROC analysis. For ADC, the horizontal thin line in graph d shows the optimal cut-point for differentiating subgroups of group A. Although a significant difference in ADC values between the two groups can be seen ($p<0.001$), an overlap zone is appreciable from 1.52 to 2.01 x $10^{-3}mm^2s^{-1}$ (area between dotted horizontal lines). Conversely, for SII, there are no overlapped values between the two groups.

FIGURE 2. Receiver operating characteristic (ROC) curves indicate the sensitivity and specificity of ADC-based differentiation between groups (A vs. B) (a) and between subgroups of group A (NT vs. TLH) (b). For each curve, the optimal cut-off value is highlighted with the relative values of sensitivity and specificity.

FIGURE 3. Graphs show for each group the relationship between SII and age for TLH/NT (a) and THY (b), and between ADC and age for TLH/NT (c) and THY (d) expressed by the Pearson's correlation coefficient. Note the significant positive relationship between each quantitative parameter and age for group A (TLH/NT; a: SII, r=0.885, $p<0.0001$; c: ADC, r=0.288, $p=0.022$), but not for group B (THY; b: SII, r=0.245, $p=0.249$; d: ADC, r=0.235, $p=0.269$). Filled circles: TLH for group A, advanced THY for group B; empty circles: NT for group A; non-advanced THY for group B.

FIGURE 4. A 41-year old woman with TLH. (a) Chemical-shift MRI shows a quadrilateral-shaped diffuse enlargement of the thymus anterior to the pulmonary trunk, with slightly convex lateral contours and a remarkable homogeneous decrease in signal intensity (arrows) on opposed-phase

images relative to in-phase images (SII=38.18%). This finding proves the presence of fat within the thymus and suggests the diagnosis of a diffusely enlarged TLH. (b) The ADC map of DW-MRI shows unrestricted diffusion (ADC=2.11 x $10^{-3}mm^2s^{-1}$) (arrows). (c) DW imaging obtained at different *b* values shows a high and homogeneous hyperintensity of the thymus at *b* value of 0 s/mm^2 that gradually decreases at *b* values of 150 and 500 s/mm^2 and is completely suppressed at the higher b value of 800 s/mm^2 (arrows). (d) Photomicrograph of a representative histological section of TLH demonstrates (left image) areas of high cellular density that contain some lymphoid follicles with germinal centres (white asterisks) and Hassall's corpuscles (arrows). The interstitial connective tissue is predominantly composed by extensive areas of fat cells (black asterisks) that decrease the cellular density per unit area. The magnification in the right image shows the morphology of a Hassall's corpuscle within a context of high cell density (Hematoxylin and eosin stain; original magnification: x40 left image, x200 right image).

FIGURE 5. A 15-year old girl with TLH. (a) Chemical-shift MRI shows a quadrilateral-shaped soft-tissue mass with slightly convex margins on the left side of the anterior mediastinum that has no apparent decrease in signal intensity (arrows) on opposed-phase images relative to in-phase images (SII=7.77%), suggesting the absence of fatty component. (b) The ADC map of DW-MRI shows unrestricted diffusion (ADC=1.86 x $10^{-3}mm^2s^{-1}$) (arrows; asterisks, aortic arch). (c) DW imaging obtained at different *b* values shows a high and homogeneous hyperintensity of the thymus at *b* value of 0 s/mm^2 that gradually decreases at *b* values of 150 and 500 s/mm^2 and is completely suppressed at the higher b value of 800 s/mm^2 (arrows). (d) Photomicrograph of a representative histological section demonstrates minimally fatty-infiltrated thymic tissue with limited areas of fat cells (black asterisk) and lymphoid follicles with prominent germinal centres (white asterisks) (Hematoxylin and eosin stain; original magnification, x40). Although the SII demonstrates a 7.77% signal intensity decrease on opposed-phase images, the degree of fatty infiltration is not sufficient to determine a visually obvious decrease of signal intensity within the soft tissue mass.

FIGURE 6. A 31-year old man with advanced THY (WHO type, B3). (a) Chemical-shift MRI shows an oval-shaped soft tissue mass in the left side of the anterior mediastinum, adjacent to the pulmonary trunk, with no change in signal intensity (arrows) on opposed-phase images relative to in-phase images (SII=1.77%), consistent with the absence of fat tissue. (b) The ADC map of DW-MRI shows restricted diffusion (arrow) that suggests high density cellular tissue (ADC=0.72 x $10^{-3}mm^2s^{-1}$). A mild bilateral pleural effusion is also seen (white asterisks). (c) DW imaging obtained at different *b* values detects a high heterogeneous hyperintensity of the lesion that is maintained at higher *b* values (arrows). (d) Photomicrograph of a representative histological section shows a tissue of high cellular density with no fat cells that is composed by medium-sized polygonal epithelial cells with mild atypia mixed with few lymphocytes (Hematoxylin and eosin stain; original magnification, x100).

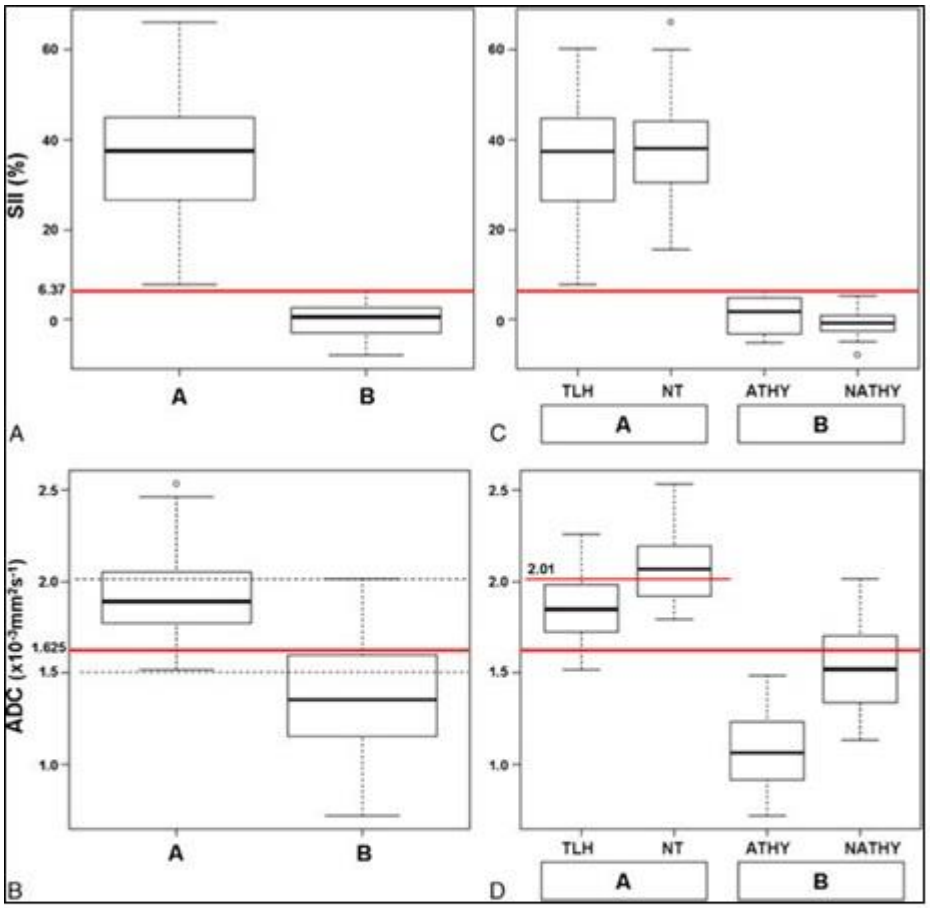
SII (%)
60
40
20
6.37
0
A
B
A
C
TLH
NT
ATHY
NATHY
A
B
ADC (x10⁻³mm²s⁻¹)
2.5
2.0
1.625
1.5
1.0
2.01
B
D

FIGURE 1

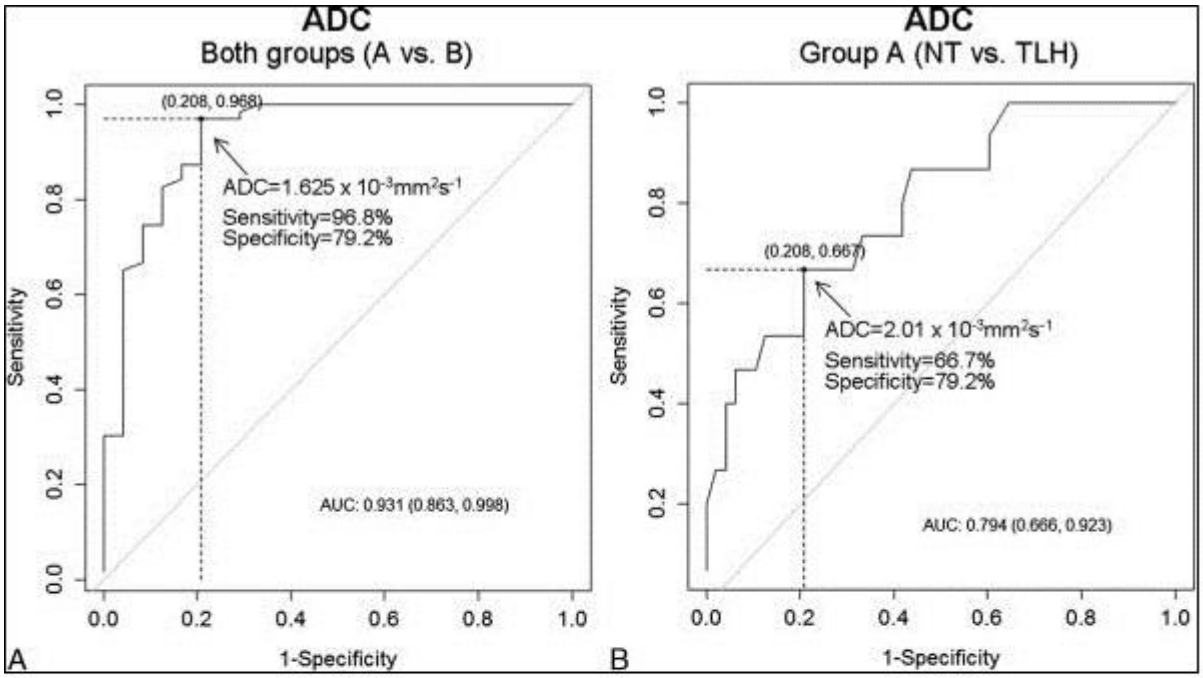
ADC
Both groups (A vs. B)
(0.208, 0.968)
ADC=1.625 x 10-3mm2s-1
Sensitivity=96.8%
Specificity=79.2%
AUC: 0.931 (0.863, 0.998)
Sensitivity
1-Specificity
A
ADC
Group A (NT vs. TLH)
(0.208, 0.667)
ADC=2.01 x 10-3mm2s-1
Sensitivity=66.7%
Specificity=79.2%
AUC: 0.794 (0.666, 0.923)
Sensitivity
1-Specificity
B

FIGURE 2

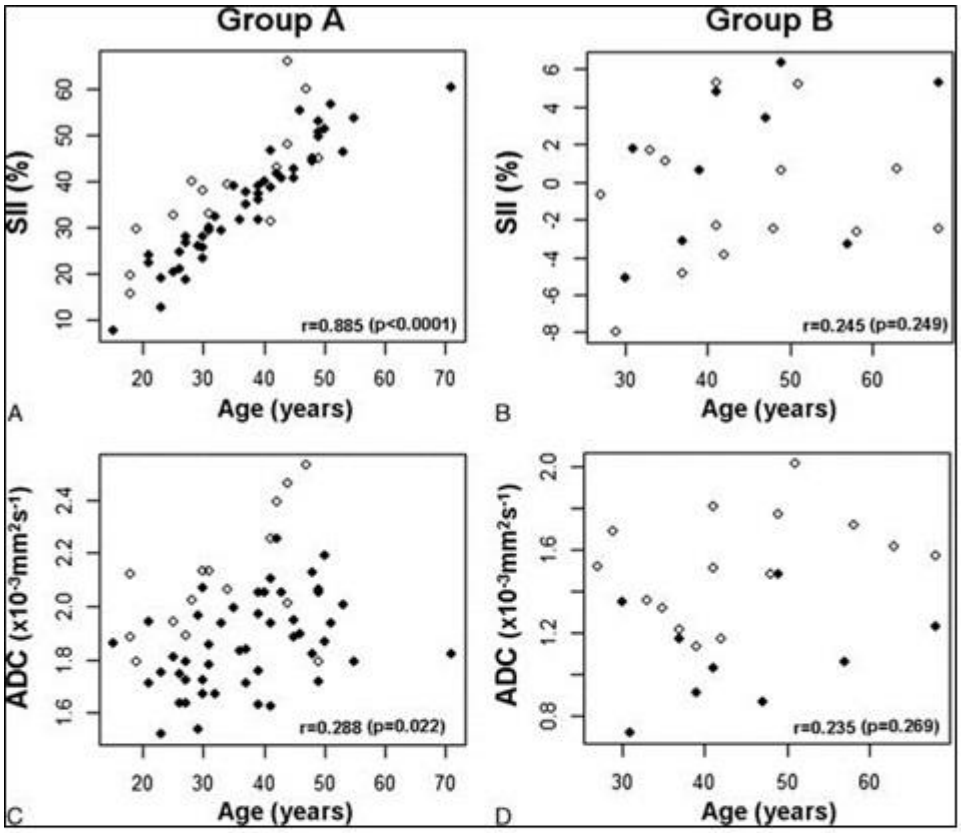
Group A
Group B
SII (%)
r=0.885 (p<0.0001)
Age (years)
A
r=0.245 (p=0.249)
B
ADC (x10-3mm2s-1)
r=0.288 (p=0.022)
C
r=0.235 (p=0.269)
D

FIGURE 3

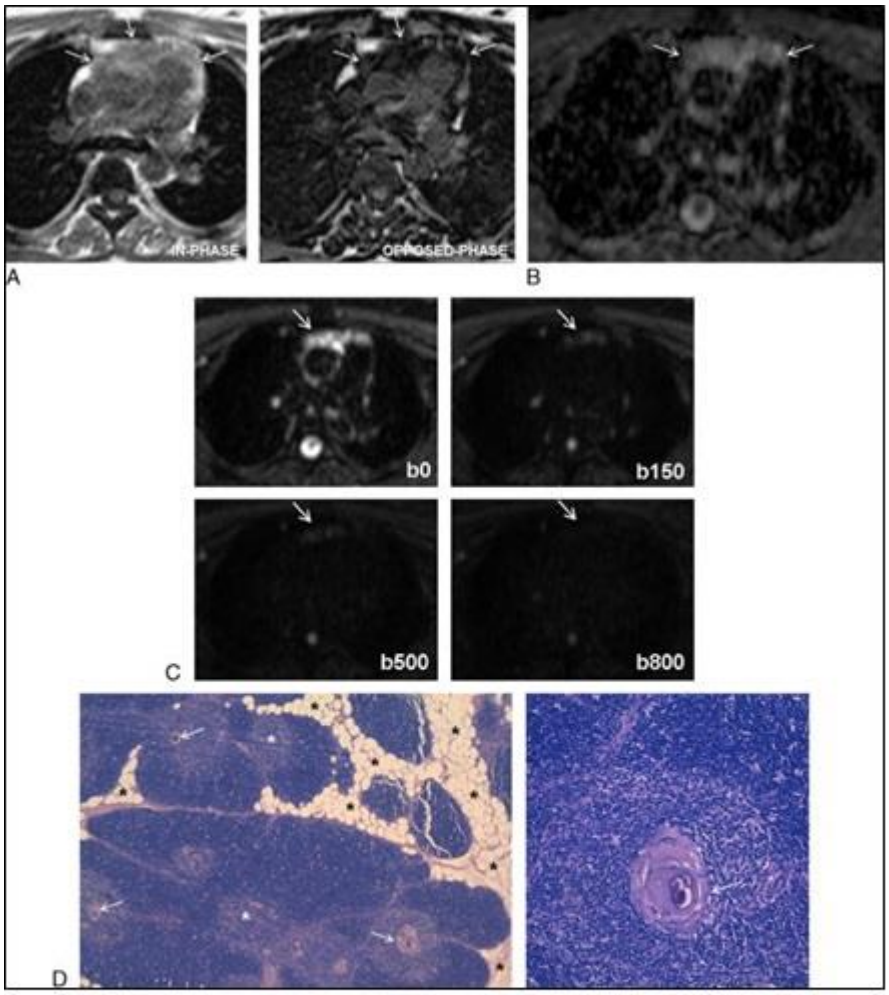

FIGURE 4

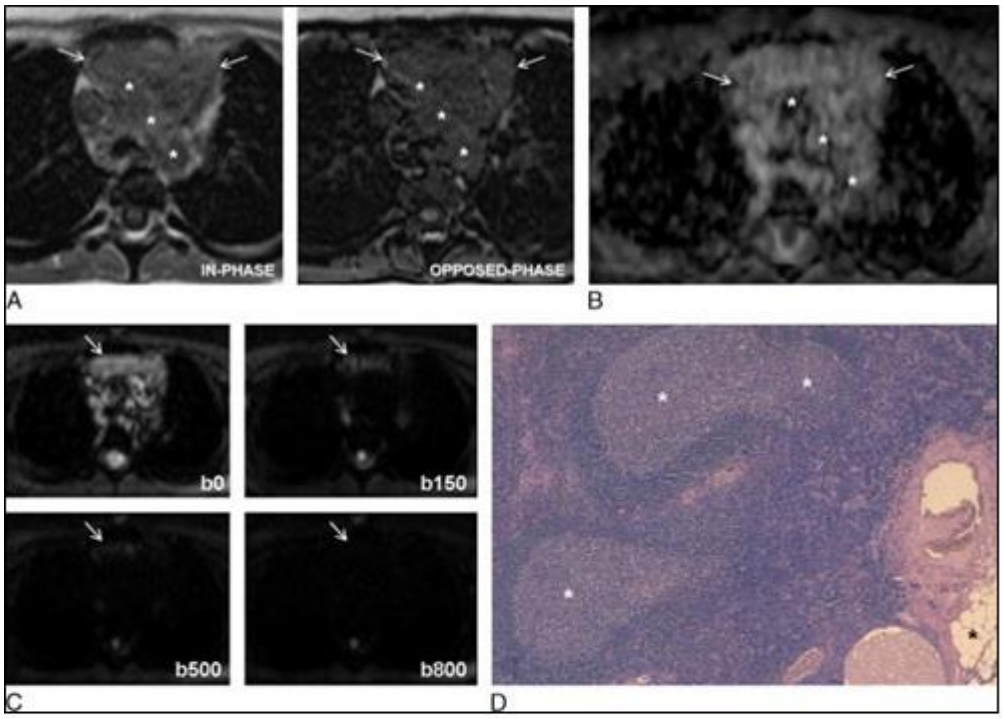

FIGURE 5

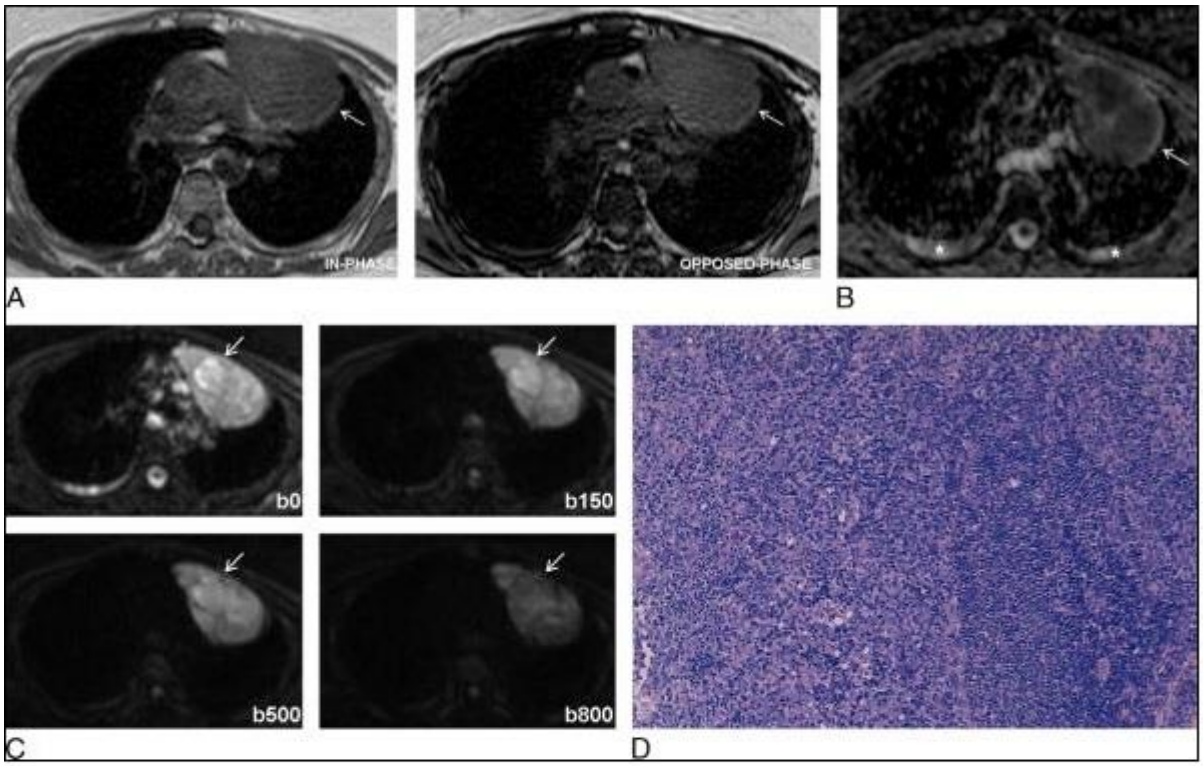

FIGURE 6